Journal of Applied Fluid Mechanics, Vol. 9, No. 3, pp. 1477-1490, 2016.
Available online at www.jafmonline.net, ISSN 1735-3572, EISSN 1735-3645.
DOI: 10.18869/acadpub.jafm.68.228.23401

Eulerian ISPH Method for Simulating Internal Flows

M. Ordoubadi, A. Farhadi, F. Yeganehdoust, H. Emdad†, M. Yaghoubi and E. Goshtasebi Rad

School of Mechanical Engineering, Shiraz University, P. O. Box 7193616548, Shiraz, Iran

†*Corresponding Author Email: hemdad@shirazu.ac.ir*

(Received June 17, 2014; accepted July 29, 2015)

ABSTRACT

In this article the possibility to use Eulerian approach in the conventional ISPH method in simulation of internal fluid flows is studied. The use of Eulerian approach makes it possible to use non-uniform particle distributions to increase the resolution in the sensitive parts of the domain, different boundary conditions can be employed more freely and particle penetration in the solid walls and tensile instability no longer require elaborate procedures. The governing equations are solved in an Eulerian framework containing both the temporal and local derivatives which make the momentum equations non-linear. Some special treatment and smaller time steps are required to remedy this non-linearity of the problem. In this study, projection method is used to enforce incompressibility with the evaluation of an intermediate velocity and then this velocity is projected on the divergence-free space. This method is applied to the internal fluid flows in a shear-driven cavity, Couette flow, a flow inside a duct with variable area and flow around a circular cylinder within a constant area duct. The results are compared with the results of Lagrangian ISPH and WCSPH methods as well as finite volume and Lattice Boltzmann grid based schemes. The results of the studied scheme have the same accuracy for velocity field and have better accuracy in pressure distribution than ISPH and WCSPH methods. Non-uniform particle distributions are also studied to check the applicability of this method and Good agreement is also observed between uniform and non-uniform particle distributions.

Keywords: Eulerian; Smoothed particle hydrodynamics; Meshfree; Incompressible flow.

1. INTRODUCTION

The Smoothed Particle Hydrodynamics (SPH) was initially developed for astrophysical problems in 1977 (Gingold and Monaghan 1977; Lucy 1977). In the past couple of decades, this meshfree Lagrangian method became popular in many branches of computational fluid dynamics, such as hydrodynamics (Lee 2007), heat transfer (Danis *et al*. 2013) and fluid-solid interaction (Amini *et al*. 2011). Traditionally, the pressure is explicitly evaluated from a weakly compressible equation of state, which enforces another time step criterion related to a virtual speed of sound. The sound speed should be at least 10 times higher than the maximum flow velocity to limit the compressibility effects below 1% (Monaghan 2005). This weakly compressible smoothed particle hydrodynamics (WCSPH) method is easy to program but it has some shortcomings. Most importantly, it requires a very small time step related to the virtual speed of sound as stated above. The next drawback is the unnatural pressure fluctuations which can cause numerical instabilities, especially when the pressure gradient is one of the main driving forces of the flow. To prevent these problems and achieve a more physical pressure field, one can use an incompressible SPH method. Cummins and Rudman (1999) implemented the projection method into the SPH for the first time to enforce incompressibility constraint. The projection method was first used to solve incompressible Navier-Stokes equations by Chorin (1968) for Eulerian grid based methods. This method uses a fractional step with the evaluation of an intermediate velocity field without considering the pressure terms initially, and then enforces compressibility by projecting this velocity field onto a divergence-free space. In a more recent study, Lee *et al*. (2008) compared the weakly compressible SPH with an Incompressible SPH method and showed that in spite of the need to solve an elliptic pressure Poisson equation in each time step, an ISPH method is in general more time efficient than a WCSPH because of larger time steps allowed.

As explained previously, the SPH is traditionally a Lagrangian method. The use of a Lagrangian method in Computational Fluid Dynamics has both advantages and disadvantages. As one of the most notable advantages, it can be stated that the capability of modeling free surfaces and

interfacial boundaries is inherently available in a Lagrangian method. In spite of these capabilities, a Lagrangian method may have some major drawbacks which have limited the use of Lagrangian meshfree methods such as SPH to some very slim range of problems. Firstly, a Lagrangian method has some serious defects concerning the boundary conditions, specially the outflow boundaries where the particles leave the domain. Secondly, Lagrangian methods have particle clustering problems (Tensile instability in SPH), which can greatly affect the stability of the method. Different solutions have been proposed to these problems, but they may cause extra programing difficulties or accuracy drawbacks. Furthermore, adaptive refinement and the use of non-uniform particle distributions are nearly impossible in a Lagrangian method because of the large movement and deformations of flows. Lastly but most importantly, because of the particle motion, the particle penetration into the solid boundary and particle escaping from the domain of computation are major concerns in the Lagrangian meshfree methods and require special boundary treatments in contrast to an Eulerian method. According to the aforementioned problems of Lagrangian methods, it seems tempting to use an Eulerian frame of reference in a meshfree method such as SPH. Danis *et al*. (2013) used ISPH and Boussinesq approximation to model transient natural convection in a square cavity for an Eulerian uniform grid, to show the upper limit of the accuracy of the SPH method in general.

Some specific particle methods facilitate both Eulerian as well as the Lagrangian formulations. The most famous is the Particle-In-Cell (PIC) method. In this method, first proposed by Harlow and his coworkers (Harlow 1957; Evans and Harlow 1957), the Lagrangian particles carry the mass and position data, while other information is saved on an Eulerian mesh. The data are transferred via interpolation between the two sets of data nodes. Some other variants of PIC method are, Fluid-in-Cell (FLIC) method (Gentry *et al*. 1966) to overcome particle distortions and Marker-and-Cell (MAC) method for modeling free surface flows (Harlow and Welch 1965).

There are also some combined Lagrangian-Eulerian grid-based methods. The Coupled Eulerian Lagrangian scheme (CEL) (Mair 1999) utilizes both Eulerian and Lagrangian methods. It is conventional in a CEL method to use Eulerian formulation in the fluid domains and Lagrangian in the solid domains. The interaction between these two domains is modeled with some kind of special interface treatment and interpolations. The Arbitrary Lagrangian Eulerian (ALE) method (Benson 1992; Hirt *et al*. 1974; Belytschko *et al*. 2000) is traditionally concerned with rezoning schemes and intends to adapt the mesh to minimize mesh distortion. In this method the Lagrangian motion is evaluated in each time step and the algorithm determines to rezone the mesh or not. These two methods have been implemented in some commercial software and are especially attractive in fluid-solid interaction (FSI) modeling. In both these methods a highly distorted mesh can still produce errors in numerical simulations and making these methods efficient is a very cumbersome task (Liu and Liu 2003).

In this study an Incompressible SPH method is used in a pure Eulerian frame of reference. The main idea behind a pure Eulerian ISPH approach is that the particles are dormant during the solution, and the transport equations are rewritten in the Eulerian reference containing both the temporal and local derivatives. This method is applied to the shear-driven cavity problem, Couette flow, a flow inside a duct with variable surface area and internal flow around a circular cylinder. The results of the cavity problem are compared with the results of Lagrangian WCSPH and ISPH methods as well as finite volume and Lattice Boltzmann schemes while the results of the Couette flow is compared to the analytical results and the variable area duct and cylinder cases are compared to finite volume results. Also, results of non-uniform particle distributions are compared to the uniform distributions to study the effects of particle distortion on this approach.

2. GOVERNING EQUATIONS

2.1 Lagrangian Formulations

In a Lagrangian Incompressible SPH method, the governing equations are the Navier-Stokes equations in the Lagrangian framework. These include the continuity and momentum equations:

$$\nabla \cdot \vec{u} = 0 \tag{1}$$

$$\frac{D\vec{u}}{Dt} = -\frac{1}{\rho}\nabla p + \nabla \cdot \left(\nu \nabla \vec{u}\right) + \vec{F} \tag{2}$$

Where $\vec{u}$, ρ , p, ν and $\vec{F}$ are the velocity vector, density, pressure, kinematic viscosity and body force vector per unit volume, respectively.

The projection method is used to calculate the pressure field and enforce incompressibility, simultaneously. This method divides the solution of momentum equation into two steps, the prediction and the projection steps (Cummins and Rudman 1999).

At the prediction step, the effect of pressure gradient is ignored and an intermediate velocity field is obtained in the *(n+1)*th time step.

$$\frac{\vec{u}^{*} - \vec{u}^{(n)}}{\Delta t} = \left[\nabla \cdot \left(\nu \nabla \vec{u}\right) + \vec{F}\right]^{(n)} \tag{3}$$

Where *(n)* refers to the *n*th time step and $\vec{u}^{*}$ is the intermediate velocity. $\vec{u}^{*}$ is zero on the stationary walls and equal to the wall velocity for the moving walls.

In the projection step, the effect of pressure gradient is included by the following equation:

$$\frac{\vec{u}^{(n+1)}-\vec{u}^{*}}{\Delta t}=\left[-\frac{1}{\rho}\nabla p\right]^{(n+1)} \tag{4}$$

One should obtain the pressure at the current time step to determine the new velocity. To this end, the divergence of Eq. (4) is taken as follows:

$$\nabla\cdot\left(\vec{u}^{(n+1)}\right)-\nabla\cdot\left(\vec{u}^{*}\right)=\Delta t\times\nabla\cdot\left[-\frac{1}{\rho}\nabla p\right]^{(n+1)} \tag{5}$$

The incompressibility in the next time step is enforced by neglecting the first term on the left hand side of this equation. It should be noticed that the intermediate velocity does not necessarily satisfy the divergence-free condition. Consequently the pressure Poisson equation is obtained:

$$\nabla^{2}p^{(n+1)}=\frac{\rho}{\Delta t}\nabla\cdot\left(\vec{u}^{*}\right) \tag{6}$$

By solving the above elliptic Poisson equation with the proper boundary conditions described in section 3.3, the pressure at the $(n+1)th$ time step is evaluated. Consequently the velocity field is projected onto the divergence-free space by using Eq. (4). It can be observed that by solving the pressure Poisson equation, the continuity constraint is readily satisfied.

2.2 Eulerian Formulations

Now consider applying the projection method to an Eulerian reference applied initially by Chorin (1968). The total derivative in the momentum equation should be written in the Eulerian format as follows:

$$\frac{D\vec{u}}{Dt}=\frac{\partial\vec{u}}{\partial t}+\vec{u}\cdot\nabla\vec{u} \tag{7}$$

And now Eq. (3) is rewritten as:

$$\frac{\vec{u}^{*}-\vec{u}^{(n)}}{\Delta t}=\left[\nabla\cdot\left(\nu\nabla\vec{u}\right)+\vec{F}-\vec{u}\cdot\nabla\vec{u}\right]^{(n)} \tag{8}$$

It should be noted here that the left hand side of Eq. (8) is the discretized form of the local derivative of velocity while the left hand side of Eq. (3) is the total derivative, giving the velocity in the direction of a path line. The convective term is regarded henceforth as another force, in addition to the viscous and body forces; hence it is only added to the prediction step. The other parts of the formulation are similar to Eqs. (4-7); keeping in mind that the velocity obtained from these equations for the Eulerian method is the velocity of fixed particles in the next time step.

The use of simple ISPH formulations will not move particles in a way to keep the volume constant. This is in contrast to the assumptions of constant volume of particles in ISPH method which will induce some accumulating numerical errors that might hamper the convergence and stability of solution. The use of an Eulerian view point in conventional ISPH methods will keep the particles fixed in space which keeps the volume of particles constant. In this manner the mentioned errors are totally omitted and good stability and convergence criteria are achieved.

3. SPH FORMULATIONS

3.1 General SPH Relations

The main idea behind the SPH methodology is that any quantity, such as α have an equivalent integral representation as:

$$\alpha\left(\vec{x}\right)=\int_{\Omega}\alpha\left(\vec{x}'\right)\delta\left(\vec{x}-\vec{x}'\right)d\vec{x}' \tag{9}$$

Where $\vec{x}$, Ω, δ and $d\vec{x}'$ are the position vector, domain of $\alpha(\vec{x})$, Dirac delta function and a differential element of space in Ω, respectively. The Dirac delta function can be approximated by a kernel or smoothing function W_h with a smoothing length of h (Gingold and Monaghan 1977; Lucy 1977). Therefore $\alpha(\vec{x})$ can be approximated as:

$$\alpha\left(\vec{x}\right)\approx\int_{\Omega}\alpha\left(\vec{x}'\right)W_h\left(\vec{x}-\vec{x}'\right)d\vec{x}' \tag{10}$$

The kernel W_h is an even, normalized function (unity condition), with the smoothing length of h. The kernel should also approach the delta function, as the smoothing length approaches to zero. The other property of the kernel function is that its value goes to zero when particle b is out of the support domain of a (compact condition). The support domain is the effective radius related directly to the value of h. Any particle b in the support domain of a, will impart forces on a. For more properties of the kernel function one can refer to references (Monaghan 2005; Liu and Liu 2003).

After some transformations (Liu and Liu 2003), equation (10) will reduce to:

$$\alpha_a=\sum_b\frac{m_b}{\rho_b}\alpha_b W_h\left(r_{ab}\right) \tag{11}$$

Where b is any particle in the support domain of the particle a, and r_{ab} is the distance from particle a to particle b. In this study the value of h is set to 1.2 times the initial particle spacing (dx).

A kernel function is generally written as:

$$W_h\left(q\right)=\frac{1}{h^{d}}f\left(q\right) \tag{12}$$

Where d is the dimension of the domain of simulation and $q=r_{ab}/h$ is the dimensionless distance between two particles. The kernel used in this study is the quartic kernel (Liu and Liu 2003; Morris 1995; Morris 1996) with the support domain of $2.5h$:

$$W_h(q)=\frac{96}{1199\times\pi\times h^2}\times \begin{cases}(2.5-q)^4-5(1.5-q)^4+10(0.5-q)^4 & 0.0\le q<0.5\\ (2.5-q)^4-5(1.5-q)^4 & 0.5\le q<1.5\\ (2.5-q)^4 & 1.5\le q<2.5\\ 0 & q\ge 2.5\end{cases} \tag{13}$$

The gradient of α is basically expressed as:

$$\nabla\alpha_a=\sum_b\frac{m_b}{\rho_b}\alpha_b\nabla_a W_h(r_{ab}) \tag{14}$$

Where $\nabla_a W_h(r_{ab})$ is the gradient of the kernel function with respect to particle *a* as:

$$\nabla_a W_h(r_{ab})=\frac{\vec{x}_a-\vec{x}_b}{r_{ab}}\frac{\partial W_h(r_{ab})}{\partial r_{ab}} \tag{15}$$

There are also other methods available to express gradients and divergences as discussed in (Liu and Liu 2003; Monaghan 2005). For example the gradient of a scalar can also be represented as:

$$\nabla\alpha_a=\rho_a\sum_b m_b\left(\frac{\alpha_a}{\rho_a^2}+\frac{\alpha_b}{\rho_b^2}\right)\nabla_a W_h(r_{ab}) \tag{16}$$

As stated in (Monaghan 2005; Lee *et al*. 2008), Eq. (16) is asymmetric, which conserves linear momentum and is employed for the pressure gradient term.

The divergence of a vector can also be represented in different styles. The relation used in this study is:

$$\nabla\cdot\vec{u}_a=-\frac{1}{\rho_a}\sum_b m_b\vec{u}_{ab}\cdot\nabla_a W_h(r_{ab}) \tag{17}$$

Where $\vec{u}_a$ is any vector such as velocity and $\vec{u}_{ab}=\vec{u}_a-\vec{u}_b$.

In an Eulerian framework, some attention should be given to the convective term in the momentum equation, since this term transforms the equations into non-linear partial differential equations. Because of this non-linearity, the discretization of this term can severely alter the numerical results. For an incompressible flow, the convective term can also be written as:

$$\vec{u}\cdot\nabla\alpha=\nabla\cdot(\alpha\vec{u})-\alpha\nabla\cdot\vec{u}=\nabla\cdot(\alpha\vec{u})-0 \tag{18}$$

It is observed in this study that discretizing the convective term in this conservative manner, gives more accurate results than when the convective term is kept in its innate form such as in Eq. (7). This is due to the fact that by using Eq. (18), the continuity equation is again satisfied. This form of the convective term can be discretized by the use of Eq. (17).

The diffusion term in the momentum equation is discretized using the relation given by Morris *et al*. (1997):

$$\nabla\cdot(\nu\nabla\vec{u})_a=\sum_b m_b\left(\frac{\rho_a\nu_a+\rho_b\nu_b}{\rho_a\rho_b}\frac{\vec{x}_{ab}\cdot\nabla_a W_h(r_{ab})}{r_{ab}^2+\eta^2}\right)\vec{u}_{ab} \tag{19}$$

Where $\eta=0.1h$ is a parameter to prevent division by zero. There are also other methods to discretize the diffusion term such as those given in (Monaghan 2005; Cleary and Monaghan 1999), but the present numerical studies showed that Eq. (19) gives better and more accurate results.

The next term that should be discretized is the Laplacian of the pressure field in Eq. (6). Higher order derivatives can be discretized using the higher order derivatives of the kernel function directly as described in Liu and Liu (2003). But this direct discretization can greatly reduce the accuracy of the numerical simulation, and a checker-board effect such as that observed in grid-based collocated methods, may prevail. Hence another method for discretization of the Laplacian is used by Cummins and Rudman (1999). In this approximation the SPH and finite difference formulations are combined to give a relation similar to the diffusion term given in Eq. (19), such as:

$$\nabla^2 p_a=\frac{2}{\rho_a}\sum_b m_b\frac{p_{ab}\vec{x}_{ab}\cdot\nabla_a W_h(r_{ab})}{r_{ab}^2+\eta^2} \tag{20}$$

In this study the pressure Poisson equation is solved using conjugate gradient method introduced by Hestenes and Stiefel (1952) with the boundary conditions described in section 3.3.

3.2 Time Step Constraint

The time step limit for this method is obtained from the criteria on the Courant and viscous conditions.

$$\Delta t=C_t\times\min\left(0.4\frac{h}{|u_{ref}|},0.125\min\frac{h^2}{\nu_a}\right) \tag{21}$$

Where u_{ref} is the reference velocity of the problem and C_t is a constant coefficient. In Lagrangian formulations C_t is set to 1, while in Eulerian formulations this parameter is set to a number lower than 1, such as 0.2. This lower requirement on time step is due to the non-linear convective term which requires a lower time step for better stability. With some numerical experiments it is observed that a value of 0.2 can give stable and accurate results for a diverse range of flow Reynolds numbers.

It should be emphasized that in a Lagrangian method another criterion limits the authorized time step, related to the Lagrangian inertial acceleration of the particles (Lee *et al*. 2008), which is disregarded in the present simulations.

3.3 Boundary Conditions

In the SPH, like any other CFD method, different methods are available to handle boundary conditions. In this study, four kinds of boundary conditions are used, namely: solid wall, periodic, velocity inlet and pressure outlet boundary conditions.

There are different boundary types in SPH to simulate solid walls, namely the use of repulsive force (Monaghan 1994), ghost or mirror particles (Cummins and Rudman 1999) and dummy particles (Shao and Lo 2003).

The repulsive force boundary condition, first proposed by Monaghan in 1994, uses forces similar to inter-molecular interactions. A force is exerted on a fluid particle having a distance r from a boundary particle, which has the form of Lennard-Jones potential. This force is increased as the distance r between a boundary and a fluid particle is decreased, preventing the fluid particles from penetrating the wall.

The mirror particle method is used to enforce the no-slip as well as the Neumann boundary conditions. In this method the particles whose support domain is truncated by a solid boundary are reflected on the other side of the wall. The mirror or ghost particles have the same pressure as their corresponding fluid particles but have velocities extrapolated from the fluid and wall velocities.

One of the sources of inaccuracy in the SPH method without any kind of kernel or gradient kernel correction is the truncation of the boundary particles. This means that, not enough particles might be present in the support domain of a fluid particle. The other method to model solid walls is the use of dummy particles. In this method several layers of stationary dummy particles are placed parallel to the boundary particles, so the support domain of the particles located close to the solid wall will not be truncated any longer. These layers of dummy particles are linked to their corresponding boundary particles and have the same pressure and velocity as their linked particles. In the present study, dummy particles are used to model solid walls. A schematic of fluid, boundary and dummy particles is shown in Fig. 1. The velocity and the intermediate velocities are held constant on the boundary particles, but their pressure is calculated from the solution of Eq. (6). Afterwards, the pressure of the dummy particles is updated to their corresponding boundary particles. In this way the Neumann boundary condition on the walls is approximated.

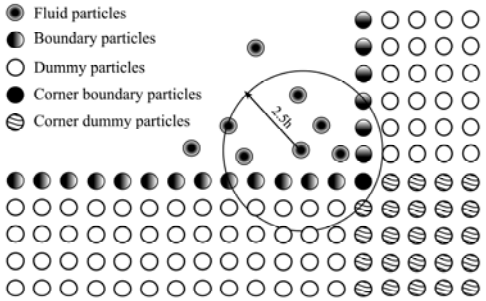

Fig. 1. Position of boundary and dummy particles with respect to fluid particles.

The periodic boundary particle in Eulerian viewpoint is straight-forward. Any fluid particle near one side of these boundaries whose support domain is truncated by periodic boundary have mirrored support domain near the other end of the domain.

Velocity inlet boundary condition used in this study also employs some layers of dummy particles which are placed outside the inlet region, and are linked with the fluid particles near the inlet. The velocity values of these fluid particles exactly located at the inlet are held constant at the desired value, but their pressures are calculated from the solution of Eq. (6). The dummy particles linked with these inlet particles are given the same velocity and pressure magnitudes.

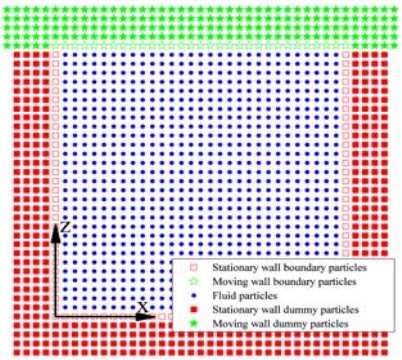

Fig. 2. The shear driven cavity with uniform particle distribution.

The pressure outlet boundary condition is generally the same as the inlet condition with some associated linked dummy particles, with the only exception that, the pressure of outlet particles are held constant while their velocity values are calculated from Eq. (4).

4. RESULTS

4.1 Shear Driven Cavity

The shear driven cavity is a benchmark problem for most of the CFD methods and simulations. The results of this study are compared with the results of Ghia *et al*. (1982) as well as Lagrangian SPH methods for the shear driven cavity for the Reynolds numbers of 100, 400 and 1000. Two sets of particle distributions of 60 by 60 and 110 by 110 particles are studied. In order to compare this method with other numerical schemes, the results of LBM study of Kumar and Agrawal (2013) are also presented for Reynolds numbers of 400 and 1000.

The cavity modeled in this study is a two dimensional 1 by 1 square domain. The domain and particle distribution is shown in Fig. 2. The flow is given constant density and the upper wall velocity of 1. The dynamic viscosity of the fluid is altered to give the desired Reynolds numbers. It should be stated that in this study, 4 dummy particles are assigned to each ordinary boundary particle. The extra column of dummy particles for the upper corners in Fig. 2 is used to prevent particle penetration in the Lagrangian simulation; and for the matter of comparison, this set-up is also used for

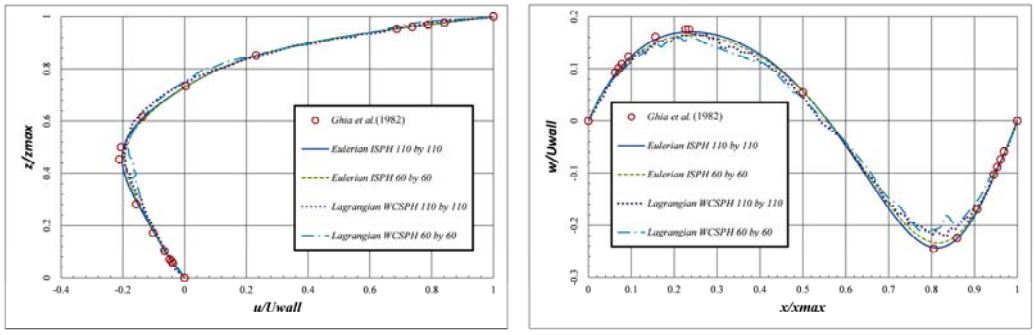

(a) (b)

Fig. 3. Velocity profiles for Reynolds number of 100 for shear driven cavity.

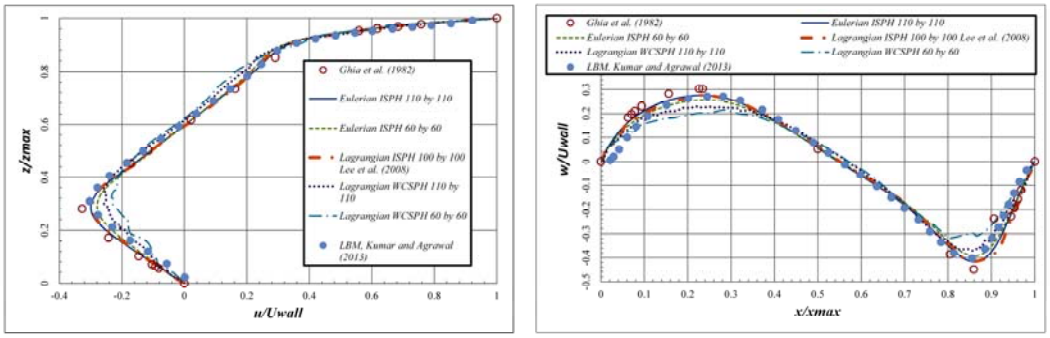

(a) (b)

Fig. 4. Velocity profiles for Reynolds number of 400 for shear driven cavity.

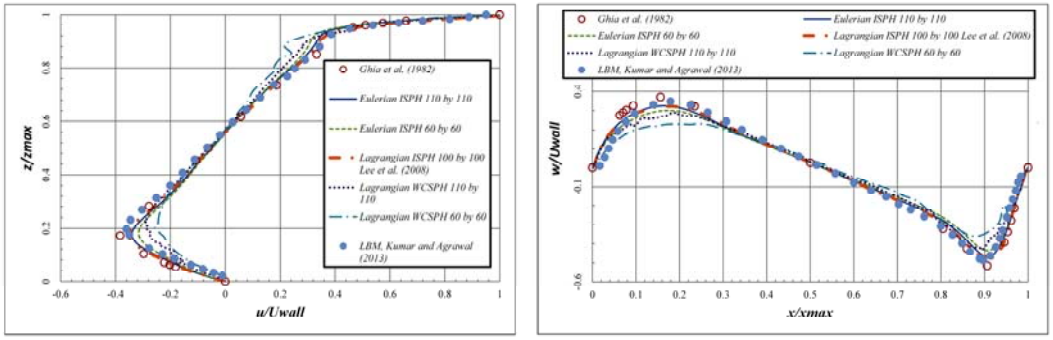

(a) (b)

Fig. 5. Velocity profiles for Reynolds number of 1000 for shear driven cavity.

the Eulerian case.

After setting up the problem and generating the required input data files and geometries with different number of particles (uniform and non-uniform distributions), the shear-driven cavity is simulated for different Reynolds numbers. These results are compared with Lagrangian WCSPH results, Lagrangian ISPH results of Lee *et al*. (2008), the FV results of Ghia *et al*. (1982) and LBM results of Kumar and Agrawal (2013).

Then, WCSPH and Eulerian ISPH for uniform particle distributions are run at Reynolds numbers of 100, 400 and 1000 and the velocity profiles along the mid horizontal and vertical lines are plotted in Figs. 3, 4 and 5, respectively. As expected, by increasing the number of particles, the accuracy of all methods is increased. For the Reynolds number of 100, the results show better agreement with FV data. At this Reynolds number, even the coarser particle distributions show accurate results. This is due to the fact that for lower Reynolds numbers, the diffusion term is dominant in the momentum equations. Also at these low Reynolds numbers, the vortex core in the cavity is much larger than those in the higher Reynolds numbers. At these vortex cores, the pressures field is smoother than the rest of the flow field which decreases the associated errors due to the pressure gradient term in the momentum equation. Consequently, decreasing the Reynolds number will increase the size of vortex core and lead to more accurate results. It is also evident from Figs. 4 and 5 that LBM shows better results in some parts of the domain while ISPH

method can capture the FV data better in other regions. It should be mentioned here that like ISPH method, numerous modifications has been performed on LBM to further increase its accuracy and performance. For example Rahmati and Ashrafizaadeh (2009) proposed a generalized LBM for incompressible fluid flow simulations.

The results of Eulerian and Lagrangian ISPH methods for constant particle resolutions are practically the same, while the WCSPH velocities are not as accurate and show spatial fluctuations, particularly for lower resolutions. It should be remarked here that, to compensate the inaccuracies related to the non-linearity of the convective terms, the same accuracy between the Eulerian and Lagrangian methods is achieved by lowering the time step in the former to about one fifth of the latter as stated in section 3.2. The low accuracy of the WCSPH is mainly due to the use of an unphysical equation of state, which leads to unreal pressure field, which in turn decreases velocity field's accuracy as was also seen in Lee (2007).

The pressure profiles at the horizontal centerline for the Reynolds number of 1000 are shown in Fig. 6. The parameter *Pmid* in the ordinate title is the reference pressure at the center of the cavity. As seen in this figure, the Eulerian pressure profiles of different number of particles are close to the finite volume result. In spite of higher particle resolution, the Lagrangian ISPH suffers in accuracy, albeit it shows good spatial stability. The result of the Lagrangian WCSPH shows spatial fluctuations in the pressure field and confirms the fact that the pressure field of a WCSPH method is unphysical. It is also evident from this figure that for the Lagrangian ISPH method, the Neumann pressure boundary condition is not satisfied near the walls which might increase the particle penetration inside the walls. This difference in the pressure field near the solid walls is mainly due to the continual movement of the fluid particles, which forces the pressure of boundary particles to change continuously, in order to match with their surrounding fluid particles' new positions. In the Eulerian and FV cases, the pressure profiles are normal to the wall surfaces, which confirm that, these methods satisfy the pressure Neumann condition.

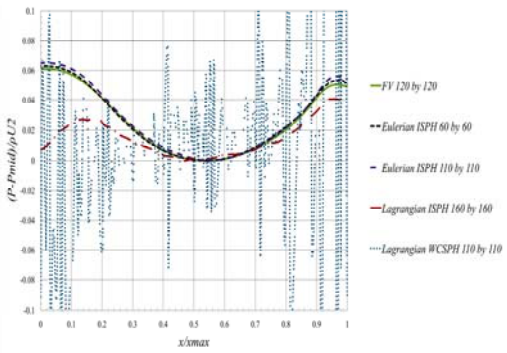

Fig. 6. Pressure profiles at the horizontal centerline for Reynolds number of 1000 for shear driven cavity.

The results of a FV laminar code, for simulation of shear-driven cavity is also used to compare the contours of constant velocities and pressures, for the Reynolds number of 1000. These contours are shown in Figs. 7, 8 and 9. The vortex core near the center and the small separation zones at the corners of the cavity are identical in the two methods.

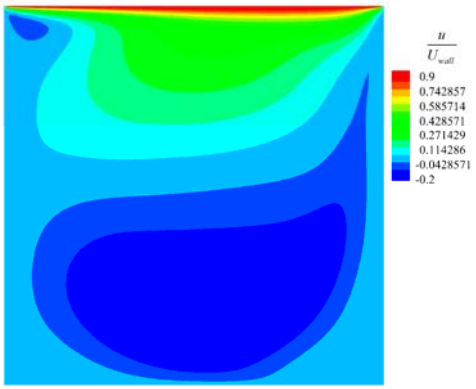

(a)

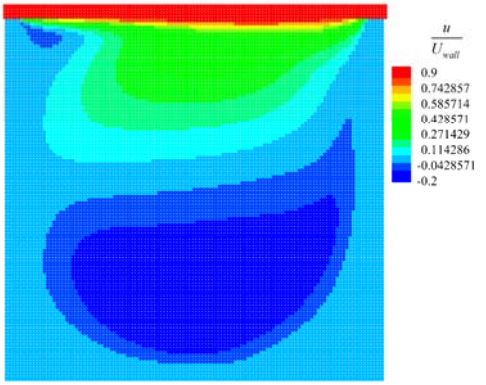

(b)

Fig. 7. Contours of x velocity (a) FV, (b) Eulerian ISPH.

To further investigate the accuracy of the results of this study the relative l^2-norm of the errors for different field variables are calculated as:

$$l^2 = \sqrt{\frac{\sum_{i=1}^{N}\left(X_{EISPH}(i) - X_{Exact}(i)\right)^2}{\sum_{i=1}^{N} X_{Exact}^2(i)}} \qquad (22)$$

Where X_{EISPH} is the relevant field variable of the Eulerian ISPH method and X_{Exact} is the field variable of the benchmark studies. The errors calculated from Eq. (22) for the velocity profiles of shear-driven cavity for Reynolds number of 1000 are shown in Table 1 and Table 2. The errors corresponding to the pressure field are also shown in Table 3. In these tables, the velocity values are compared to the results of Ghia *et al*. (1982), while the pressure results are compared to the results of the FV code used.

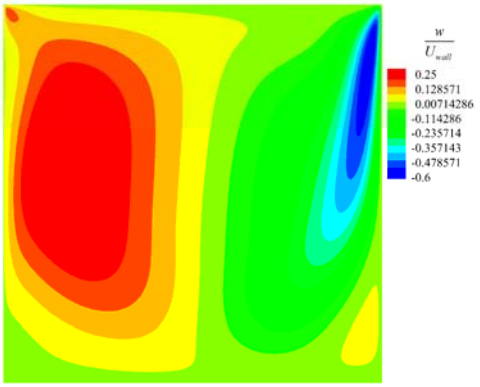

(a)

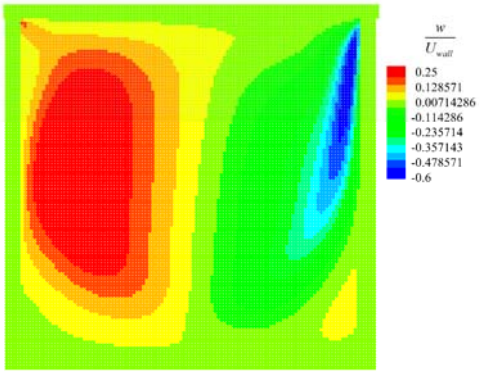

(b)

Fig. 8. Contours of z velocity (a) FV, (b) Eulerian ISPH.

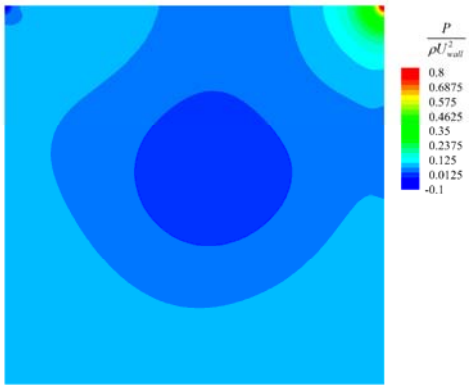

(a)

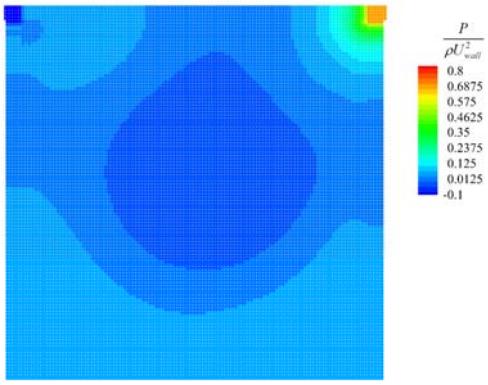

(b)

Fig. 9. Contours of normalized pressure (a) FV, (b) Eulerian ISPH.

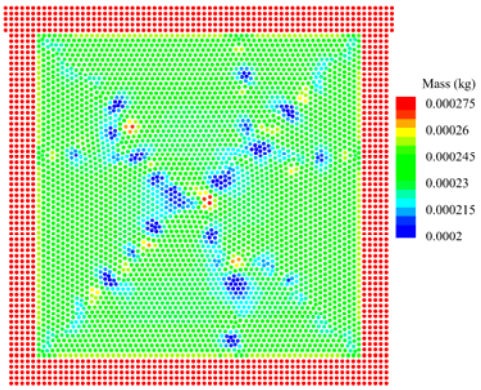

Fig. 10. Non-uniform particle distribution, colored with the mass of the particles obtained from Equation (23).

Table 1 Horizontal velocity l^2 -norm errors, compared to Ghia *et al.* (1982)

Eulerian ISPH, 110 by 110 particles	0.169
Eulerian ISPH, 60 by 60 particles	0.189
Lagrangian ISPH, Lee *et al*. (2008)	0.134

Table 2 Vertical velocity l^2 -norm errors, compared to Ghia *et al.* (1982)

Eulerian ISPH, 110 by 110 particles	0.230
Eulerian ISPH, 60 by 60 particles	0.325
Lagrangian ISPH, Lee *et al*. (2008)	0.266

Table 3 Pressure l^2 -norm errors, compared to FV results

Eulerian ISPH, 110 by 110 particles	0.077
Lagrangian ISPH, Lee *et al*. (2008)	0.564

It is clear from these tables that the velocity profiles of the Lagrangian ISPH method is more accurate than the Eulerian method, which is due to the extra numerical deficiency associated with the convective terms in Eulerian methodology. On the other hand, the pressure profile of the Eulerian method is about 7 times more accurate than the Lagrangian method. As stated before, the continual movement of particles in the Lagrangian methods causes this large pressure error, especially near the solid walls.

In order to check the generality of this Eulerian approach, some non-uniform particle distributions are also studied for shear driven cavity problem. Two sets of non-uniform particle distributions are studied for Reynolds number of 1000, one with 5465 and the other with 13765 particles, which can be compared with the results of uniform distributions of 60 by 60 (4771 particles) and 110 by 110 (14171 particles), respectively. The non-uniform distribution of 5465 particles is shown in Fig. 10, colored with the mass of the particles. The non-uniform distribution is obtained by placing

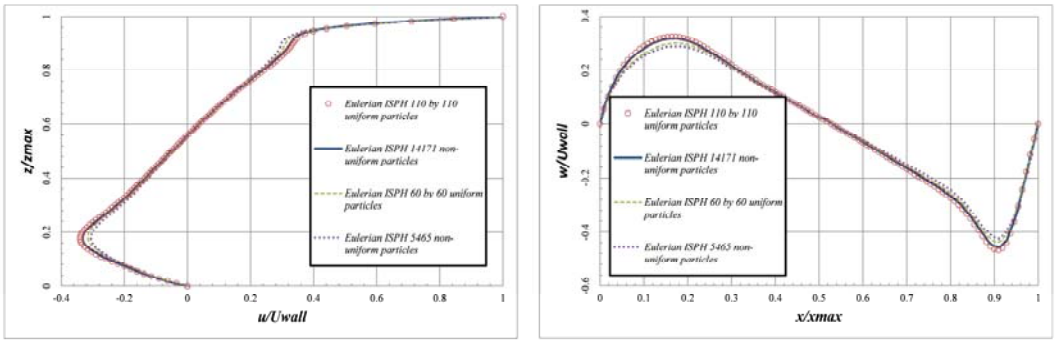

Fig. 11. Velocity profiles for the non-uniform particle distributions for Reynolds number of 1000.

particles on the nodes of a finite volume unstructured grid containing triangular cells. The major difference between uniform and non-uniform distributions is the method to calculate the initial mass of the particles. In both cases masses are calculated from the density and volume of the particles. In the uniform distribution the volume of the particles is dx^2, where dx is the initial particle spacing. The volume calculation of particles in the non-uniform distribution requires further attention. In this study, the volume of particles is calculated directly from the SPH formulations. Consider α as the inverse of volume of particle *a* in Eq. (11). With some simple substitutions, Eq. (23) is obtained for the volume of particle *a*.

$$\forall_a = \frac{1}{\sum_b W_h(r_{ab})} \tag{23}$$

The mass of particles can be evaluated from the volumes obtained from Eq. (23) at the beginning of solution, and are constant during the rest of the solution.

The velocity profiles of the non-uniform particle distributions are shown in Fig. 11. A slight difference is present between the uniform and non-uniform distributions with comparable number of particles. This slight difference originates from the non-uniformity of particles in the kernel support domains which in turn leads to lower accuracy in the calculation of derivatives using SPH discretization. This non-uniformity mostly affects the non-linear convective terms. The use of kernel corrections (Liu and Liu 2003) will decrease the inaccuracies associated with distorted particle distributions.

4.2 Couette Flow

Couette flow with no pressure gradient is also studied to check the unsteady accuracy of Eulerian approach. The case is consisted of two parallel plates each with length l=0.6 m and separated by a distance d=0.1 m from each other, while the upper wall is given a fixed horizontal velocity U_0=0.001 m/s. The kinematic viscosity of the flow is set to $\nu = 1\times10^{-3}$ m^2/s, corresponding to Reynolds number of 0.1. The exact solution to this problem is:

$$u(z,t) = \frac{U_0}{d}z + \sum_{n=1}^{\infty}\frac{2U_0}{n\pi}(-1)^n \sin\left[\frac{n\pi}{d}z\right]e^{\left[-\nu\frac{n^2\pi^2}{d^2}t\right]} \tag{24}$$

Where t is time in seconds.

A particle distribution of 180×30 particles with initial particle spacing of 3.4×10^{-3}m is used for this simulation. The left and right extremes of the domain are periodic boundary conditions. At t=0, the fluid is stationary and the upper wall is suddenly moved with a constant velocity of U_0. At about t=3 sec, the fluid will reach a steady state solution.

Because of the fact that pressure gradient is neglected in this specific case, the results of an incompressible and weakly compressible simulation should be the same in similar spatial and temporal resolutions. The results of an Eulerian approach compared to a Lagrangian one on the other hand might be different because of the non-linearity of the former approach. The horizontal velocity profiles at 4 different times of the solution are compared to the exact solutions in Fig. 12. Good agreement between these results is observed. There is a slight deviation between the Eulerian SPH and the exact results, far from the steady state solution, while the steady state results show the best agreement with the exact solution.

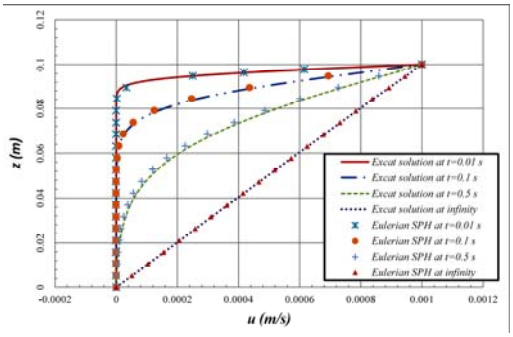

Fig. 12. Horizontal velocity profiles of Couette flow at different times.

4.3 Variable Area Duct

The internal flow inside a duct with variable flow area is also analyzed using the Eulerian ISPH scheme. The geometry used is shown in Fig. 13. D

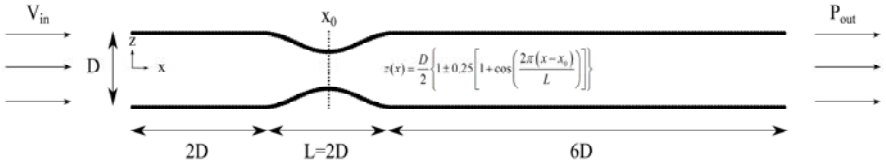

Fig. 13. Variable area duct.

is the internal spacing of the duct, L is the total length of the contracted region and x_0 is the horizontal position of the center of this region. The contracted region is created from a cosine profile shown in the figure.

In the test case studied, D is set to 0.1 m, kinematic viscosity is set to 0.0001 m^2/s, the outlet pressure is held constant and equal to 0 and a fully developed laminar profile is assumed for the inlet velocity condition with mean velocity of 0.3 m/s. With these properties the Reynolds number of the case studied is 300, which is low enough to be within the laminar regime and high enough to stay out of the creeping conditions; which makes it possible to observe the separation regions in the diverging section of the duct.

Two particle distributions are used for this case. The first one has a total of 5296 particles, with a uniform particle spacing of 0.005 m. The second distribution has a total number of 5312 particles and has the same resolution outside the contracted region as the first distribution, but has variable particle spacing in vertical direction in this region. This vertical particle spacing decreases with the decreasing of the flow area. These resolutions are good enough to capture the reverse flow generated after the diverging section of the duct. The contracted region of these two distributions is compared in Fig. 14.

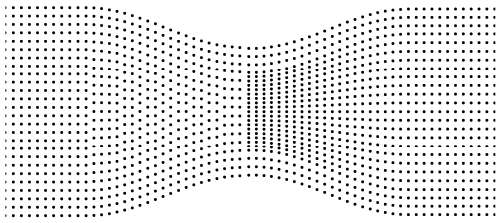

Fig. 14. Uniform (left) and non-uniform (right) particle distributions of the variable area duct.

The results of the variable area duct are compared to the FV solution. The internal flow simulated has Reynolds number of 300, guaranteeing the existence of reverse flows near the contraction. The horizontal velocity and pressure contours of the Eulerian ISPH method are compared to the results of the FV method in Figs. 15 and 16, respectively. Good agreement is observed with the results of the FV simulation. The horizontal velocity profiles of the Eulerian ISPH method with uniform particle distribution are also compared to FV results at three positions, x=3D, x=4D and x=10D in Fig. 17. These positions correspond to the center of the contraction region, end of the contraction region and the outlet of the duct, respectively. It is clear from the horizontal velocity profiles at x=4D, that the Eulerian method captures the reverse flow after diverging section of the duct. It should be noted here that in the Lagrangian simulations of this problem with these low number of particles, a strong void appears after the diverging section of the flow, causing the solution of Poisson equation unstable and severely error-prone. To solve this issue the number of particles should be increased to more than 20 thousand particles, increasing the CPU time dramatically and making the solution practically unacceptable. In an Eulerian approach on the other hand, the particles are fixed in the domain, and this problem is fully resolved even with low number of particles. It is also evident from these profiles that, at higher velocities near the lower flow areas, Eulerian method has larger deficiency. This is mainly due to the fact that in these regions the effect of the convective term in Eq. (8) has become more dominant, hence the numerical error associated with this term is also increased.

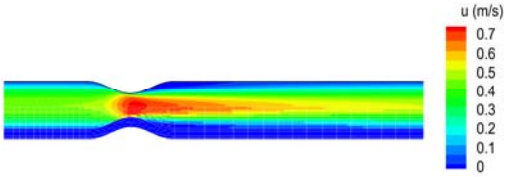

Fig. 15. Contours of constant horizontal velocity of variable area duct, FV (up) and EISPH (down).

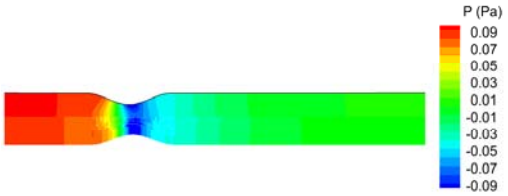

Fig. 16. Contours of constant pressure of variable area duct, FV (up) and EISPH (down).

The velocity profiles of uniform and non-uniform particle distributions at x=3D are compared in Fig. 18. The accuracy of the non-uniform distribution is slightly increased. The relative l^2-norm errors of the profiles in Fig. 18 with respect to the finite volume data are 0.0622 and 0.0469 for uniform and non-uniform spacing distributions, respectively. Flow around a circular cylinder within a constant area duct

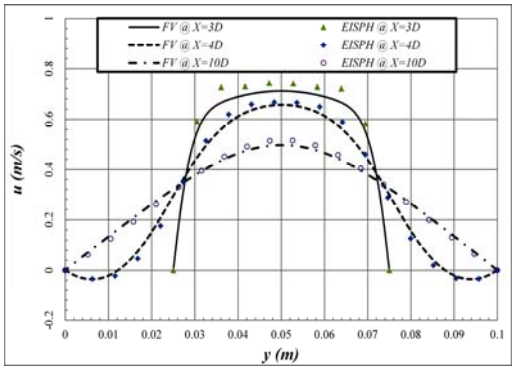

Fig. 17. Horizontal velocity profiles of flow inside a variable area duct in different positions.

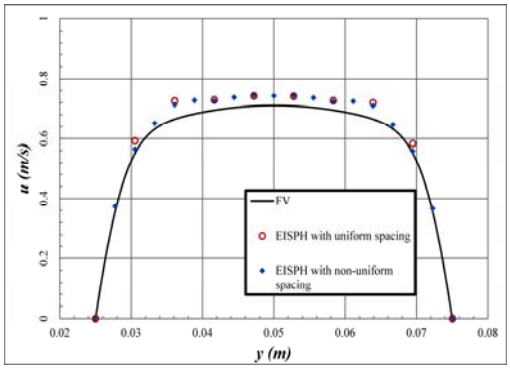

Fig. 18. Horizontal velocity for uniform and non-uniform distributions at x=3D.

The next case studied is laminar flow around a circular cylinder within a duct. The geometry considered is shown in Fig. 19. D is set to 0.1 m and fluid flows with constant density of 1.0 kg/m^3 flows from the left side with uniform velocity of 0.2 m/s and exits from the right side at constant pressure of 0.0 Pa. The flow is contained between two parallel plates 5D apart. The kinematic viscosity is 0.01 m^2/s, resulting in a Reynolds number of 10 with respect to the duct width (5D). Two different particle distributions are studied. The first one has a constant and uniform particle spacing of 0.01 with a total number of 6326 particles. The second one is consisted of a multi-resolution particle distribution with finer particle spacing around the cylinder with a total number of 6618 particles. These two particle distributions are shown in Fig. 20 (dummy particles of the cylinder wall are not shown).

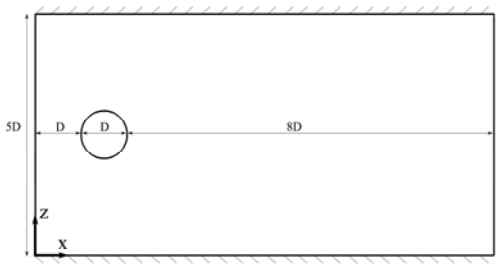

Fig. 19. Geometry of internal flow around circular cylinder between two parallel plates.

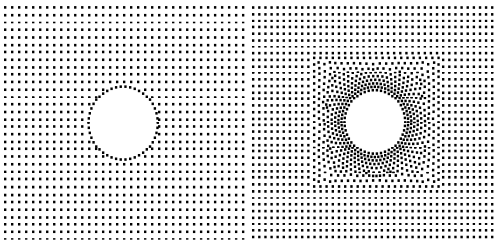

Fig. 20. Uniform and non-uniform particle distributions around the cylinder.

Here, the Eulerian ISPH results are compared to two resolutions of Lagrangian ISPH (LISPH), as well as the results of the finite volume code. The contours of constant horizontal velocity and pressure of the uniform distribution are compared to finite volume data in Figs. 21 and 22, respectively. A small difference is observable between the two results. The location of the separation on the cylinder surface is nearly at 90 degrees in both cases. It is also observed that magnitudes of horizontal velocity in EISPH are slightly larger than those of FV in the central regions of the duct. This is in part due to the use of specific pressure boundary condition explained in section 3.3 in which the pressure of the outlet dummy particles is held constant and equal to their corresponding boundary particles. Hence near the outlet boundary, pressure gradient is nearly zero which will create an adverse artificial force. In order to circumvent this issue, one can extrapolate dummy particles' pressure values from their boundary particles. As this small error does not affect the flow near the cylinder's surface, the dummy particles' are held at constant pressure in the current simulation.

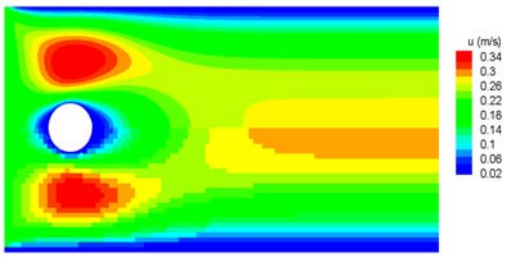

Fig. 21. Contours of constant horizontal velocity of flow around a circular cylinder, FV (up) and EISPH (down).

Fig. 22. Contours of constant pressure of flow around a circular cylinder, FV (up) and EISPH (down).

The profiles of horizontal velocity at vertical line passing through the center of the cylinder (x=1.5D) are shown in Fig. 23. The velocity profiles are practically the same for the Eulerian ISPH with uniform and non-uniform particle distributions and the Lagrangian ISPH methods, while they all have a slight underestimation of the maximum velocity compared to the finite volume result. As seen in Fig. 23, both EISPH and LISPH methods show acceptable accuracy in prediction of velocity at the position shown. They both predict the increase of velocity magnitude in vicinities above and below the cylinder, because of the concentration of streamlines.

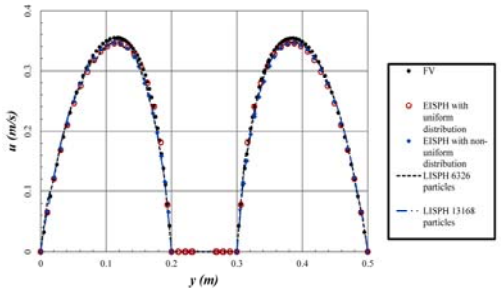

Fig. 23. Profiles of horizontal velocity at x=1.5D for flow around a cylinder.

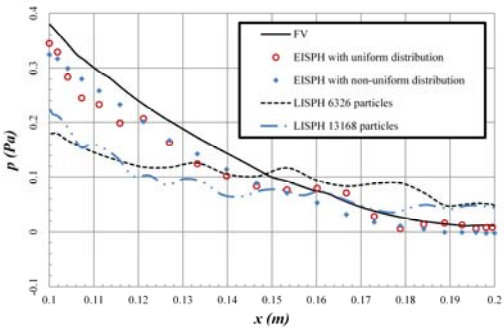

Fig. 24. Pressure on the surface of the cylinder.

The pressure on the cylinder surface is also shown in Fig. 24. The EISPH with uniform and non-uniform distributions show better accuracy with respect to finite volume results, while both resolutions of the LISPH methods have larger inaccuracies. The smooth decrease of pressure values from the front of the cylinder to the wake region behind it, is evident in the EISPH results; while LISPH has some fluctuations in pressure magnitudes even though it shows a decreasing trend. Even the LISPH with 13168 particles cannot reach the accuracy of EISPH results. It can be concluded that Lagrangian and Eulerian ISPH methods show good accuracy in velocity fields in simulation of flow around bluff bodies. But, the solution of the pressure field is not the same between two methods. The pressure field obtained with Eulerian ISPH shows better accuracy even though it might have smaller number of particles. This difference is again caused by the continual movement of the particles around the body in the Lagrangian ISPH. The Lagrangian flow around bluff bodies causes to create some kind of no-particle-region behind the body, where adverse pressure gradients are dominant as is evident in Fig. 25 showing the particle distribution at the wake of the cylinder in the Lagrangian ISPH method with 6326 particles. This lack of enough particles around the solid wall of the body causes the solution of Poisson equation, error prone and in some severe cases, completely unstable. In order to solve this issue very large number of particles should be used, which increases the solution time of even some simple scenarios dramatically. Of course at such a small Reynolds number as 10, this phenomenon is not so severe. At larger Reynolds numbers the particles completely exits the wake behind cylinder, creating a void, which causes the solution of Poisson equation to diverge.

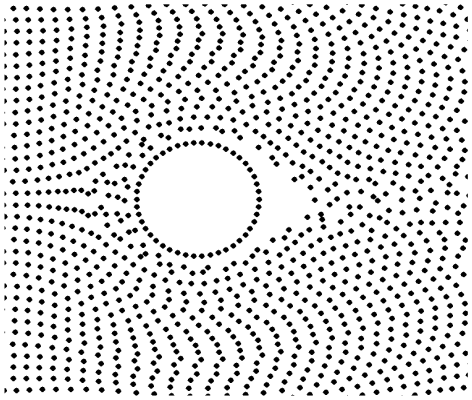

Fig. 25. Void created at the wake of the flow in LISPH method, Re = 10.

5. CONCLUSIONS

In this study, the possibility to use the Eulerian approach in the incompressible smoothed particle hydrodynamics for simulating internal flows is considered. This approach is applied to a 2-D lid-driven cavity problem for different particle resolutions and Reynolds numbers as well as Couette flow problem, flow in a duct with variable area and flow around a circular cylinder inside a constant area duct. The results are compared with the results of Lagrangian WCSPH, Lagrangian ISPH and FV methods. The main points concluded from this study are summarized in the following paragraphs.

1. The velocity profiles of the Eulerian and Lagrangian ISPH methods are practically the same, but the velocity profiles of the Lagrangian WCSPH method are not as accurate.

2. The pressure profiles of the Eulerian ISPH show great agreement with the FV results, while the Lagrangian ISPH method results show some inaccuracy especially near the solid walls and the Lagrangian WCSPH results are completely fallacious.

3. The required time step associated with the Eulerian ISPH method is around one fifth of the Lagrangian ISPH. This lower time step originates

from the non-linear convective term present in the Eulerian scheme.

4. Some non-uniform particle distributions are used to study the effects of non-uniformity of the particles on the accuracy of the simulations. The non-uniform results showed small inaccuracies compared to the results of the uniform particle distributions.

5. In internal flow simulations where the pressure field is one of the major results required from the problem, the use of Eulerian approach in an available ISPH program significantly increases the accuracy in pressure fields.

6. The Eulerian method can make use of a diverse range of boundary conditions which are presently challenging in Lagrangian SPH methods.

7. The Eulerian approach of the ISPH method is not useable for simulations concerning free surfaces or multiphase flows, which is the main advantage of SPH method over mesh based schemes.

8. Non-uniform particle distribution with stretching can also be used to increase the resolution in the sensitive regions of the flow field.

9. Because this method is still a meshfree method, programming for unstructured distributions is not different from the structured and uniform distributions, while it is a cumbersome task to program a finite volume solver to work with an unstructured grid.

10. This scheme is comparable in accuracy to other computational methods such as LBM.

ACKNOWLEDGMENTS

This study is partially supported by Iran's National Elite Foundation.

REFERENCES

Amini, Y., H. Emdad and M. Farid (2011). A new model to solve fluid–hypo-elastic solid interaction using the smoothed particle hydrodynamics (SPH) method. *European Journal of Mechanics - B/Fluids* 30,184-194.

Belytschko, T., W. K. Liu and B. Moran (2000). *Nonlinear Finite Elements for Continua and Structures.* West Sussex : Wiley.

Benson, D. J. (1992). Computational methods in Lagrangian and Eulerian hydrocodes. *Computer Methods in Applied Mechanics and Engineering* 99, 235–394.

Chorin, A. J. (1968). Numerical solution of the Navier–Stokes equations. *Mathematics of Computation* 22, 745–762.

Cleary, P. W. and J. J. Monaghan (1999). Conduction modeling using Smoothed Particle Hydrodynamics. *Journal of Computational Physics* 148, 227–264.

Cummins, S. J. and M. Rudman (1999). An SPH projection method. *Journal of Computational Physics* 152, 584–607.

Danis, M. E., M. Orhan and A. Ecder (2013). ISPH modelling of transient natural convection. *International Journal of Computational Fluid Dynamics* 27, 15–31.

Evans, M. W. and F. H. Harlow (1957). The Particle-In-Cell method for hydrodynamic calculations. *Los Alamos Scientific Laboratory report LA-2139*.

Gentry, R.A., R.E. Martin and B.J. Daly (1966). An Eulerian differencing method for unsteady compressible flow problems. *Journal of Computational Physics* 1,87–118.

Ghia, U., K. Ghia and C. Shin (1982). High-Re solutions for incompressible flow using the Navier-Stokes equations and a multigrid method. *Journal of Computational Physics* 48, 387–411.

Gingold, R. A. and J. J. Monaghan (1977). Smoothed particle hydrodynamics-theory and application to non-spherical stars. *Monthly Notices of the Royal Astronomical Society* 181, 75–389.

Harlow, F. H. (1957). Hydrodynamic problems involving large fluid distortions. *Journal of the Association for Computing machinery* 4, 137–142.

Harlow, F. H. and J. E. Welch (1965). Numerical calculation of time-dependent viscous incompressible flow of fluid with free surface. *Physics of Fluids* 8, 2182–2189.

Hestenes, M. R. and E. Stiefel (1952). Methods of conjugate gradients for solving linear systems. *Journal of Research of the Bureau of Standards* 49, 409–436.

Hirt, C. W. ,A. A. Amsden and J. L. Cook (1974). An arbitrary Lagrangian-Eulerian computing method for all flow speeds. *Journal of Computational Physics* 14, 227–253.

Kumar, A. and S. P. Agrawal (2013). Mathematical and simulation of lid driven cavity flow at different aspect ratios using single relaxation time lattice boltzmann technique. *American Journal of Theoretical and Applied Statistics* 2, 87-93.

Lee, E. S. (2007). *Truly incompressible approach for computing incompressible flow in SPH and comparisons with the traditional weakly compressible approach*. Ph. D. thesis, University of Manchester.

Lee, E. S., C. Moulinec, R. Xu, D. Violeau , D. Laurence and P. Stansby (2008). Comparisons of weakly compressible and truly incompressible algorithms for the SPH mesh free particle method. *Journal of Computational Physics* 227, 8417–8436.

Liu, G. R. and M. B. Liu (2003). Smoothed particle hydrodynamics: a meshfree particle method. Singapore, World Scientific Publishing.

Lucy, L. B. (1977). A numerical approach to the

testing of the fission hypothesis. *The Astronomical Journal* 82, 1013–1024.

Mair, H. U. (1999). Hydrocodes for structural response to underwater explosions. *Shock and Vibration* 6, 81–92.

Monaghan, J. J. (1994). Simulating free surface flows with SPH. *Journal of Computational Physics* 110,399–406.

Monaghan, J. J. (2005). Smoothed particle hydrodynamics. *Reports On Progress in Physics* 68, 1703–1759.

Morris, J. P. (1995). A Study of the Stability Properties of SPH. *Monash Applied Mathematics Reports and Preprints* 1-4.

Morris, J. P. (1996). *Analysis of smoothed particle hydrodynamics with applications*. Ph. D. thesis, Monash University.

Morris, J. P., P. J. Fox and Y. Zhu (1997). Modeling low reynolds number incompressible flows using SPH. *Journal of Computational Physics* 136, 214–226.

Rahmati, A. R. and M. Ashrafizaadeh (2009). A Generalized Lattice Boltzmann Method for Three-Dimensional Incompressible Fluid Flow Simulation. *Journal of Applied Fluid Mechanics* 2, 71-96.

Shao, S. and E. Y. M. Lo (2003). Incompressible SPH method for simulating Newtonian and non-Newtonian flows with a free surface. *Advances in Water Resources* 26, 787–800.